Inorganica Chimica Acta 379 (2011) 70–75

Contents lists available at SciVerse ScienceDirect

Inorganica Chimica Acta

journal homepage: www.elsevier.com/locate/ica

2-(R-*1H*-Benzoimidazol-2-yl)-6-(1-aryliminoethyl)pyridyliron(II) dichlorides: Synthesis, characterization and the ethylene oligomerization behavior

Liping Zhang [a,b], Xiaohua Hou [a,b], Jiangang Yu [b], Xia Chen [a,*], Xiang Hao [b], Wen-Hua Sun [b,*]

[a] *School of Chemistry and Chemical Engineering, Shanxi University, Taiyuan 030006, China*
[b] *Key Laboratory of Engineering Plastics and Beijing National Laboratory for Molecular Science, Institute of Chemistry, Chinese Academy of Sciences, Beijing 100190, China*

ARTICLE INFO

Article history:
Received 21 May 2011
Received in revised form 7 September 2011
Accepted 16 September 2011
Available online 29 September 2011

Keywords:
2-Benzimidazol-2-yl-6-iminopyridine
Iron complex
Ethylene oligomerization

ABSTRACT

Iron(II) dichloride complexes bearing 2-(methyl-substituted *1H*-benzoimidazol-2-yl)-6-(1-aryliminoethyl)pyridines (**Fe1**–**Fe6**) or 2-(chloro-substituted *1H*-benzoimidazol-2-yl)-6-(1-aryliminoethyl)pyridines (**Fe7**–**Fe12**) were synthesized and characterized by FT-IR and elemental analysis. Single crystal X-ray crystallographic analyses revealed that complexes **Fe2** and **Fe3** possessed a distorted square-pyramidal geometry at iron. Upon activation with either MAO or MMAO, all iron pro-catalysts showed good activities toward ethylene oligomerization with high selectivity for α-olefins and high *K* values. The influence of the reaction conditions and the nature of the ligands on the catalytic performance of these iron complexes were investigated.

© 2011 Elsevier B.V. All rights reserved.

1. Introduction

Over the past decade or so, iron pro-catalysts for ethylene activation have attracted increased attention, both in academic and industrial research [1–8], primarily due to the emergence of highly efficient systems containing the 2,6-diiminopyridyl ligand set [9–11]. Subsequently, the number of research papers in the area mushroomed, with much work done on varying the 2,6-diiminopyridine substituents and using various reaction conditions [12–16], as well as synthesizing unsymmetrical 2,6-diiminopyridines [17–22]. Indeed, numerous iron complexes have been explored with various alternate tridentate ligand sets such as N^N^O [23], N^P^N [24], P^N^N [25,26], and most importantly alternative N^N^N models [27–42]; the latter have also been the focus of our investigations [31–42]. Significant advantages have been exhibited by iron pro-catalysts, such as high efficiency, price (cheap) and environmental-friendly iron precursors. Moreover, the ability to form a wide variety of vinyl-type products as indicated by the oligomers and polymers that have obtained to-date. Recently, iron pro-catalysts bearing 2-(benzimidazole)-6-(1-aryliminoethyl)pyridine derivatives were shown to exhibit high activities in ethylene oligomerization [37–39]; ligand modification was conducted at the 1-substituent position of the imidazole ring within the benzimidazole. Furthermore, 2-(benzimidazole)-6-(1-aryliminoethyl)pyridines were modified with substituents at the benzo-ring of the benzimidazole, and the nickel pro-catalysts thereof [43,44] showed interesting results in ethylene oligomerization [45–47]. As a consequence, the title iron complexes were synthesized and characterized. When activated with either methylaluminoxane (MAO) or modified methylaluminoxane (MMAO), all iron pro-catalysts showed high catalytic activity in ethylene oligomerization.

2. Results and discussion

2.1. Synthesis and characterization of the title complexes

The ligands, as prepared by our previous procedure, possessed two isomers in a 3:2 M ratio, *viz.* 2-(7-methyl-*1H*-benzoimidazol-2-yl)-6-(1-aryliminoethyl)pyridines (major) and 2-(4-methyl-*1H*-benzoimidazol-2-yl)-6-(1-aryliminoethyl)pyridines (minor, **L1**–**L6**) [43], and 2-(6-chloro-*1H*-benzoimidazol-2-yl)-6-(1-aryliminoethyl)pyridines (major) and 2-(5-chloro-*1H*-benzoimidazol-2-yl)-6-(1-aryliminoethyl)pyridines (minor, **L7**–**L12**) [44]. The stoichiometric reaction of the respective 2-(R-*1H*-benzoimidazol-2-yl)-6-(1-aryliminoethyl)pyridines and $FeCl_2 \cdot 4H_2O$ in ethanol precipitated a blue powder of the corresponding 2-(R-*1H*-benzoimidazol-2-yl)-6-(1-aryliminoethyl)pyridyliron dichlorides (**Fe1**–**Fe12**) in good to high yield (60–92%) at room temperature (Scheme 1).

All iron complexes were air-stable in the solid state, and elemental analytical data confirmed their formula; they slowly turn from blue to yellow in solution on exposure to air (oxidation of Fe^{2+}). Compared with the IR spectra of the free ligands, for which the C=N stretching frequencies are in the range of 1639–

---

* Corresponding authors. Tel.: +86 10 62557955; fax: +86 10 62618239 (W.-H. Sun).
E-mail address: whsun@iccas.ac.cn (W.-H. Sun).

0020-1693/$ - see front matter © 2011 Elsevier B.V. All rights reserved.
doi:10.1016/j.ica.2011.09.035

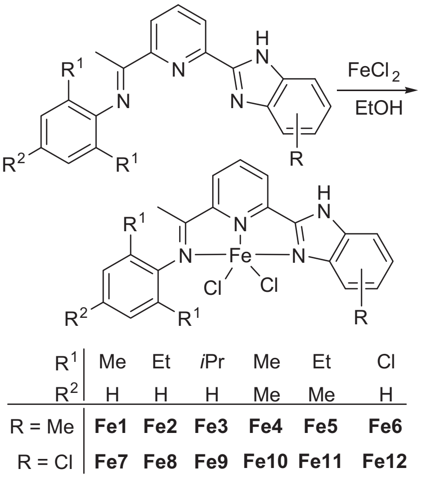

R^1	Me	Et	iPr	Me	Et	Cl
R^2	H	H	H	Me	Me	H
R = Me	**Fe1**	**Fe2**	**Fe3**	**Fe4**	**Fe5**	**Fe6**
R = Cl	**Fe7**	**Fe8**	**Fe9**	**Fe10**	**Fe11**	**Fe12**

Scheme 1. Synthesis of iron complexes.

1650 cm^{-1}, the C=N stretching vibrations of the complexes **Fe1**–**Fe12** were shifted toward lower frequencies (1591–1600 cm^{-1}) and with reduced intensity of the absorptions, indicating effective coordination between the imino group and the iron center. To confirm their unambiguous molecular structures, single crystals of the representative complexes **Fe2** and **Fe3** were obtained by slow diffusion of diethyl ether into methanol solutions under a nitrogen atmosphere. It is necessary to mention that there are present two isomers of the iron complex in the solid state, which are consistent with two isomers of the ligand. The major isomers of both iron complexes **C2** and **C3** have the coordinated ligands with the methyl group (linked to the carbon C4) on benzimidazole ring far to iron atom; meanwhile the minor isomers of them have the ligands with the methyl group (linked to the carbon C1) on the benzimidazole ring close to iron atom.

The structure of complex **Fe2** (Fig. 1) is best described as distorted square-pyramidal, with the basal plane composed of N2, N3, N4, and Cl1. The iron atom deviates from the plane (N2, N3 and N4) by 0.157 Å, whereas Cl1 deviates by 0.999 Å on the opposite side. There are slight differences between Fe–Cl1 (2.2634(11) Å) and Fe–Cl2 (2.3774(11) Å) due to the apical elongation in the square-pyramidal geometry. The Fe–N3 (pyridyl) (2.153(3) Å) bond is shorter (by about 0.09 Å) than the Fe–N4 (imino) (2.240(3) Å) bond and only a little shorter than the Fe–N2 (benzimidazole) (2.173(3) Å). The equatorial plane (which formed by N3, Cl1 and Cl2) is almost perpendicular to the benzimidazole ring with the dihedral angle of 84.6°, and has a dihedral angle of 134.4° with the 2,6-diethylphenyl group. A similar geometry was also observed for related iron(II) complexes [37–39]. Selected bond lengths and angles are listed in Table 1.

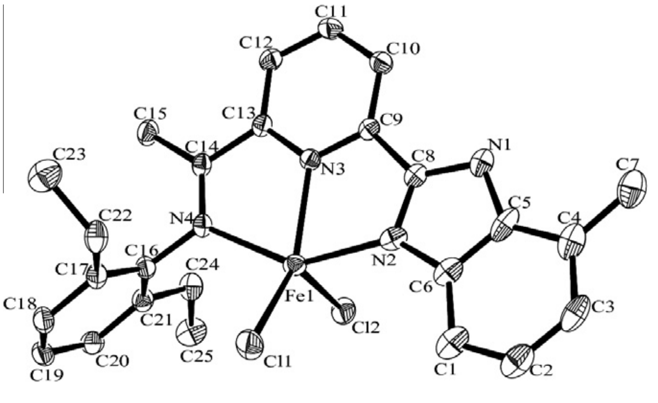

Fig. 1. ORTEP molecular structure of **Fe2**. Thermal ellipsoids are shown at 30% probability. Hydrogen atoms and solvent molecules have been omitted for clarity.

With similar structural features to **Fe2**, the molecular structure of complex **Fe3** is shown in Fig. 2. According to Table 1, the bond lengths of Fe–N and Fe–Cl are close to those of **Fe2**. Slightly different to **Fe2**, the basal plane (N2, N3, N4, Cl1) in **Fe3** is more flat with less deviation (0.201 Å) of Cl1 to the plane (N2, N3, N4), whilst the iron atom deviates from the plane (N2, N3, N4) by 0.371 Å to the opposite side. The two nitrogen atoms (N2 and N4) occupy the axial sites with the bond angle of 143.34(9)° for N2–**Fe1**–N4. The dihedral angles between the equatorial plane (which formed by N3, Cl1 and Cl2) with the phenyl ring and the benzimidazole plane are 52.4° and 86.2°, respectively. Similar to the structure of **Fe2**, longer Fe–N bonds than observed in nickel complexes bearing the same ligands are observed in **Fe3**. Selected bond lengths and angles are listed in Table 1.

2.2. Ethylene oligomerization

Based on the series of ligands used, the complexes were classified into two groups, namely **Fe1**–**Fe6** and **Fe7**–**Fe12**. Complexes **Fe1** and **Fe7** were selected as the representative pre-catalysts and were investigated for determining the optimum reaction conditions at 30 atm of ethylene using the co-catalyst methylaluminoxane (MAO) or modified methylaluminoxane (MMAO). The predominant products isolated were oligomers in the range C4–C28, with very high selectivity observed for linear α-olefins. Interestingly, the most suitable co-catalyst for **Fe1**–**Fe6** was MMAO, whilst MAO was preferable for **Fe7**–**Fe12**. The distribution of oligomers obtained in all cases resembled the Schulz–Flory distribution, which is characterized by the constant *K*, where *K* represents the probability of chain propagation (*K* = rate of propagation/((rate of propagation) + (rate of chain transfer) = (moles of Cn + 2)/(moles of Cn)) [45–49] and the *K* values are determined by the molar ratio of the C14 and C12 fractions. The results are summarized in Tables 2 and 3, respectively.

2.2.1. Ethylene oligomerization by ***Fe1–Fe6***

As shown in Table 2 (entries 1–2 in Table 2), pro-catalyst **Fe1** performed with higher activity using MMAO than with MAO, therefore further detailed investigations of **Fe1** with MMAO were carried out by changing the Al/Fe molar ratios (entries 2–7 in Table

Table 1
Selected bond lengths (Å) and angles (°) for complexes **Fe2** and **Fe3**.

	Fe2	**Fe3**
Bond length (Å)		
Fe–N2	2.173(3)	2.183(3)
Fe–N3	2.153(3)	2.147(3)
Fe–N4	2.240(3)	2.244(2)
Fe–Cl1	2.2634(11)	2.2696(12)
Fe–Cl2	2.3774(11)	2.3936(12)
N1–C8	1.343(4)	1.346(4)
N2–C8	1.331(5)	1.325(4)
N4–C14	1.284(5)	1.287(4)
Bond angle (°)		
N2–Fe–N3	73.87(11)	73.79(10)
N2–Fe–N4	145.58(11)	143.34(9)
N3–Fe–N4	72.22(11)	72.39(9)
N2–Fe–Cl1	102.93(9)	105.58(8)
N3–Fe–Cl1	145.07(8)	155.09(8)
N4–Fe–Cl1	101.39(8)	99.22(7)
Cl–Fe–Cl2	114.65(5)	106.98(4)
N2–Fe–Cl2	93.34(8)	96.01(8)
N3–Fe–Cl2	100.27(8)	97.78(8)
N4–Fe–Cl2	98.26(8)	102.12(7)

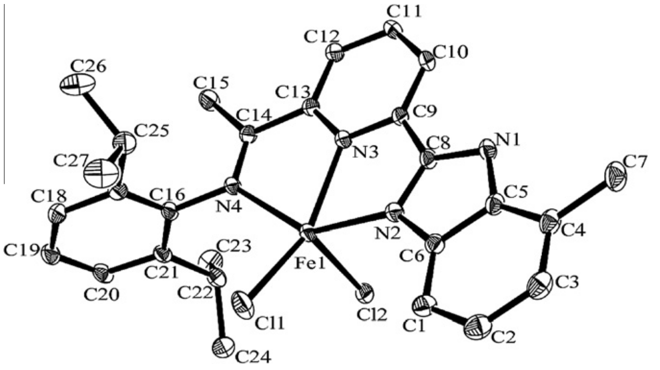

Fig. 2. ORTEP Molecular structure of **Fe3**. Thermal ellipsoids are shown at 30% probability. Hydrogen atoms and solvent molecules have been omitted for clarity.

2) and the reaction temperature (entries 5 and 8–11 in Table 2). The optimum activity was observed at the Al/Fe molar ratio of 200 at 30 °C. Iron pro-catalysts are required to be activated with a suitable amount of co-catalyst; a lower Al/Fe ratio would mean the MMAO present would be consumed by impurities in the solvent, whilst higher Al/Fe molar ratios would increase the amount of isobutyl groups from MMAO and hinder the insertion reaction of ethylene at the active species [37,48]. At room temperature, a lower catalytic activity (entry 8 in Table 2) was observed than that at 30 °C (entry 5 in Table 2), indicating the enhanced thermal stability of the active species present. However, deactivation was evident at higher reaction temperatures (entries 9–11 in Table 2), indicating unstable active species or partially lower solubility of the ethylene in solution. Under the optimum condition (Al/Fe molar ratio of 200 and 30 °C), iron pro-catalysts **Fe2**–**Fe6** were investigated (entries 12–16 in Table 2).

The nature of the ligands was found to affect the catalytic behavior of the iron pro-catalysts **Fe1**–**Fe6** (entries 5 and 12–16 in Table 2), and variation of the R^1 and R^2 substituents resulted in changes in catalytic performance. Regarding the steric hindrance of the R^1 group, pro-catalysts having a less bulky R^1 group led to an

Table 2
Ethylene oligomerization with **Fe1**–**Fe6**.[a]

Entry	Complex	Co-cat.	Al/Fe	*T* (°C)	*K*	Activity[b]	Oligomer distribution[c]				
							C4/ΣC	C6/ΣC	C8/ΣC	⩾C10/ΣC	α-Olefin (%)
1	**Fe1**	MAO	1000	30	0.92	0.7	44.5	9.6	29.3	16.6	93.7
2	**Fe1**	MMAO	1000	30	0.95	1.8	49.5	12.6	6.3	31.6	95.2
3	**Fe1**	MMAO	500	30	0.67	2.5	50.4	18.3	8.9	22.4	95.0
4	**Fe1**	MMAO	250	30	0.63	6.0	38.4	23.9	13.4	24.3	98.0
5	**Fe1**	MMAO	200	30	0.69	18.6	40.2	25.1	13.3	21.4	98.2
6	**Fe1**	MMAO	150	30	0.67	9.6	40.0	23.0	7.5	29.5	98.8
7	**Fe1**	MMAO	100	30	0.83	3.2	74.8	5.2	2.9	17.1	97.5
8	**Fe1**	MMAO	200	20	0.76	11.3	45.1	18.3	11.4	25.2	96.3
9	**Fe1**	MMAO	200	40	0.70	5.0	39.6	21.4	13.2	25.8	96.6
10	**Fe1**	MMAO	200	60	0.72	4.2	34.4	22.0	13.2	30.0	97.5
11	**Fe1**	MMAO	200	80	0.90	3.4	51.1	19.0	9.6	20.3	96.8
12	**Fe2**	MMAO	200	30	0.52	8.0	54.2	24.2	10.1	11.5	97.5
13	**Fe3**	MMAO	200	30	0.61	4.4	61.9	21.7	6.8	9.6	98.0
14	**Fe4**	MMAO	200	30	0.66	30.3	41.0	28.8	14.9	15.3	>99
15	**Fe5**	MMAO	200	30	0.63	11.9	40.3	24.8	13.7	21.2	>99
16	**Fe6**	MMAO	200	30	0.52	1.8	39.1	25.8	13.3	21.8	98.1

[a] Conditions: 5 μmol Fe, 30 min, 30 atm ethylene; 100 mL toluene.
[b] 10^5 g mol^{-1}(Fe) h^{-1}.
[c] Determined by GC.

Table 3
Ethylene oligomerization with **Fe7**–**Fe12**.[a]

Entry	Complex	Co-cat.	Al/Fe	*T* (°C)	*K*	Activity[b]	Oligomer distribution[c]				
							C4/ΣC	C6/ΣC	C8/ΣC	⩾C10/ΣC	α-Olefin (%)
1	**Fe7**	MMAO	1000	30	0.56	0.6	41.1	21.1	10.3	27.5	95.5
2	**Fe7**	MAO	1000	30	0.75	4.1	34.2	20.6	11.2	34.0	96.3
3	**Fe7**	MAO	500	30	0.72	9.6	33.6	20.9	12.5	33.0	98.0
4	**Fe7**	MAO	350	30	0.71	13.2	34.4	21.6	12.8	31.2	98.2
5	**Fe7**	MAO	250	30	0.71	28.2	32.2	22.3	13.7	31.8	98.6
6	**Fe7**	MAO	200	30	0.72	7.5	36.8	20.4	11.9	30.9	99.0
7	**Fe7**	MAO	150	30	0.77	2.7	28.3	13.0	10.4	48.3	98.4
8	**Fe7**	MAO	250	20	0.65	25.3	30.9	20.7	12.4	36.0	98.8
9	**Fe7**	MAO	250	40	0.69	24.1	33.6	22.8	13.2	30.4	98.5
10	**Fe7**	MAO	250	60	0.67	7.5	35.5	24.1	12.3	28.1	98.2
11	**Fe7**	MAO	250	80	0.75	5.1	28.7	28.3	14.9	28.1	97.8
12	**Fe8**	MAO	250	30	0.76	8.0	33.5	20.8	12.0	33.7	>99
13	**Fe9**	MAO	250	30	0.79	6.7	38.5	22.0	11.9	27.6	>99
14	**Fe10**	MAO	250	30	0.72	12.9	39.3	20.9	11.6	28.2	98.0
15	**Fe11**	MAO	250	30	0.63	7.5	34.4	28.6	15.1	21.9	>99
16	**Fe12**	MAO	250	30	0.52	5.6	49.2	17.1	9.0	24.7	97.3

[a] Conditions: 5 μmol Fe, 30 min, 30 atm ethylene, 100 mL toluene.
[b] 10^5 g mol^{-1}(Fe) h^{-1}.
[c] Determined by GC.

Table 4
Crystal data and structure refinement for **Fe2** and **Fe3**.

	Fe2	**Fe3·CH$_3$OH**
Formula	$C_{25}H_{26}Cl_2FeN_4$	$C_{28}H_{34}C_{l2}FeN_4O$
Formula weight	509.25	569.34
T (K)	173(2)	173(2)
λ (Å)	0.71073	0.71073
Crystal system	orthorhombic	triclinic
Space group	*Pbca*	$P\bar{1}$
a (Å)	15.341(3)	8.7280(17)
b (Å)	15.906(3)	9.4894(19)
c (Å)	19.334(4)	17.988(4)
α (°)	90	89.70(3)
β (°)	90	77.66(3)
γ (°)	90	69.20(3)
V (Å^3)	4717.8(16)	1356.4(5)
Z	8	2
D_{calc} (g cm^{-3})	1.434	1.394
μ (mm^{-1})	0.887	0.781
F(000)	2112	596
Crystal size (mm)	0.22 × 0.22 × 0.08	0.13 × 0.11 × 0.02
θ range (°)	2.11–27.46	2.30–27.47
Limiting indices	$-18 \leqslant h \leqslant 19$, $-20 \leqslant k \leqslant 20$, $-20 \leqslant l \leqslant 25$	$-11 \leqslant h \leqslant 11$, $-12 \leqslant k \leqslant 12$, $-23 \leqslant l \leqslant 23$
Reflections collected	31141	18403
Independent reflections (R_{int})	5383 (0.0401)	6214 (0.0549)
Number of parameters	289	363
Completeness to θ (%)	99.7	99.9
Goodness-of-fit (GOF) on F^2	0.932	1.102
Final *R* indices [$I > 2\sigma(I)$]	$R_1 = 0.0695$, $wR_2 = 0.1873$	$R_1 = 0.0617$, $wR_2 = 0.1431$
R indices (all data)	$R_1 = 0.0719$, $wR_2 = 0.1896$	$R_1 = 0.0747$, $wR_2 = 0.1431$
Maximum/minimum $\Delta\rho$[a] (e Å^{-3})	1.079 and −0.858	0.419 and −0.542

enhanced activity and the order **Fe1** > **Fe2** > **Fe3** (entries 5, 12, 13, Table 2), and also **Fe4** was higher than **Fe5** (entries 14 and 15 in Table 2). Such phenomena were reversed to the previously catalytic observations by their analogues [37,38], indicating the characteristic feature of the current pre-catalysts containing an active N–H group within the *1H*-benzoimidazol-2-yl substituent. Moreover, **Fe4** and **Fe5** with additional methyl groups exhibited higher activities than did the corresponding analogues of **Fe1** and **Fe2**. Such phenomena were in agreement with other catalytic systems of iron pro-catalysts [36–38] due to their enhanced solubility. The procatalyst **Fe6** (entry 16 in Table 2) containing ligands with chloro-substituents showed a lower activity, consistent with a lower solubility of a metal complex ligated by halo-organic compounds [37–39,43,44]. In all cases, the oligomers were mostly linear α-olefins with high *K* values.

2.2.2. Ethylene activation for the *Fe7–Fe12*

Employing MAO or MMAO as co-catalyst (entries 1–2 in Table 3), pro-catalyst **Fe7** showed a higher activity with MAO than with MMAO. Changing the molar ratio of MAO to iron (entries 2–7 in Table 3), the best activity was observed at the Al/Fe molar ratio of 250 (entry 5 in Table 3). In the temperature range of 20–80 °C (entries 5, 8–11 in Table 3), the optimum reaction temperature was found to be 30 °C. Therefore, the pro-catalysts **Fe8**–**Fe12** were investigated with the Al/Fe molar ratio of 250 at 30 °C (entries 12–16 in Table 3). All iron pro-catalysts exhibited high activities towards ethylene oligomerization and with high selectivity for linear α-olefins and high *K* values.

For the influence of the R^1 substituents, similar trends for **Fe7**–**Fe12** were observed as seen in the series **Fe1**–**Fe6**; the catalytic activities were in the order **Fe7** > **Fe8** > **Fe9** (entries 5, 12 and 13 in Table 3), and **Fe10** > **Fe11** (entries 14 and 15 in Table 3). However, the R^2 substituent did not show any positive effects. With additional methyl groups, the catalytic activities were decreased with the observed order **Fe7** > **Fe10** and **Fe8** > **Fe11**. Again, pro-catalyst **Fe12** (entry 16 in Table 3) bearing 2,6-dichlorophenyl groups exhibited a lower activity.

Although both series of iron pro-catalysts herein performed with high activities for ethylene oligomerization, they did not surpass the high activities associated with other iron pro-catalysts [31,32,37–39]. Interestingly, the substituents which were modified were far from the metal center, the synergic catalytic performances of iron pro-catalysts with different co-catalysts were changed with the influences of R (methyl- or chloro-) substituents in their ligands. Promisingly, such modified iron pro-catalysts showed high selectivity for linear α-olefins with high *K* values. Thus these systems hold further promise for exploration for industrial applications.

3. Conclusion

Iron(II) dichlorides bearing 2-(methyl substituted *1H*-benzoimidazol-2-yl)-6-(1-aryliminoethyl)pyridines (**Fe1**–**Fe6**) and 2-(chloro substituted *1H*-benzoimidazol-2-yl)-6-(1-aryliminoethyl)pyridines (**Fe7**–**Fe12**), were synthesized and characterized. X-ray crystallographic studies on the iron complexes **Fe2** and **Fe3** revealed a distorted square-pyramidal geometry at iron. When activated with MMAO, pro-catalysts **Fe1**–**Fe6** gave high activities ($\leqslant 1.86 \times 10^6$ g·(mol Fe)$^{-1}$ h^{-1}) in ethylene oligomerization, whilst pro-catalysts **Fe7**–**Fe12** showed high activities (2.82×10^6 g·(mol Fe)$^{-1}$ h^{-1}) upon treatment with MAO. All oligomers produced were in the range of C4–C28 with very high selectivity for linear α-olefins and high *K* values.

4. Experimental

4.1. General considerations

All manipulations of air- and moisture-sensitive compounds were performed at nitrogen atmosphere using standard Schlenk techniques. Toluene was refluxed over sodium-benzophenone and distilled under argon prior to use. Methylaluminoxane (MAO, a 1.46 M solution in toluene) and modify methylaluminoxane (MMAO, 1.93 M in heptane, 3A) were purchased from Akzo Nobel Corp. Other reagents were purchased from Aldrich or Acros Chemicals. IR spectra were recorded on a Perkin–Elmer System 2000 FT-IR spectrometer. Elemental analysis was carried out using an Flash EA 1112 micro-analyzer. GC analysis was performed with a Varian CP-3800 gas chromatograph equipped with a flame ionization detector and a 30 m (0.2 mm i.d., 0.25 μm film thickness) CP-Sil 5 CB column. The yield of oligomers was calculated by referencing with the mass of the solvent on the basis of the prerequisite that the mass of each fraction was approximately proportional to its integrated areas in the GC trace. Selectivity for the linear α-olefin was defined as (amount of linear α-olefin of all fractions)/(total amount of oligomer products) in percentage.

2-(Methyl-substituted *1H*-benzoimidazol-2-yl)-6-(1-aryliminoethyl)pyridines were prepared according to our previous work [43], and 2-(chloro-substituted *1H*-benzoimidazol-2-yl)-6-(1-aryliminoethyl)pyridines were prepared according to our previous work [44].

4.2. Synthesis of tridentate iron complexes ***Fe1–Fe12***

The complexes **Fe1–Fe12** were synthesized by the reaction of $FeCl_2{\cdot}4H_2O$ with the corresponding ligands in ethanol. A typical synthetic procedure for **Fe1** can be described as follows: the ligand **L1** (0.12 g, 0.35 mmol) and $FeCl_2{\cdot}4H_2O$ (0.069 g, 0.35 mmol) were added to a Schlenk tube, followed by the addition of freshly distilled ethanol (5 mL) with rapid stirring at room temperature. The solution turned green immediately, and a blue precipitate was formed. The reaction mixture was stirred for 12 h, and then the precipitate was washed with diethyl ether twice and dried to give the pure product as a blue powder in 91.3% yield. IR (KBr; cm^{-1}): 3325.1 (m), 2971.3 (w), 1591.5 (vs), 1472.5 (s), 1206.4 (s), 1041.4 (m), 790.8 (s), 762.6 (s). *Anal.* Calc. for $C_{23}H_{22}Cl_2FeN_4$ (480.1): C, 57.41; H, 4.61; N, 11.64. Found: C, 57.78; H, 4.23; N, 11.38%.

Data for **Fe2** are as follows. Yield: 86.4%. IR (KBr; cm^{-1}): 3396.3 (m), 3051.0 (m), 2970.4 (m), 1594.9 (vs), 1448.3 (s), 1378.0 (s), 1318.5 (s), 1202.0 (s), 792.2 (s), 751.9 (s). *Anal.* Calc. for $C_{25}H_{26}Cl_2FeN_4$ (508.1): C, 58.96; H, 5.15; N, 11.00. Found: C, 58.69; H, 5.20; N, 10.75%.

Data for **Fe3** are as follows. Yield: 88.3%. IR (KBr; cm^{-1}): 3484.8 (s), 3058.4 (m), 2966.0 (m), 1591.0 (vs), 1472.0 (s), 1444.9 (s), 1319.5 (s), 1202.7 (s), 816.6 (m), 766.7 (s), 746.1 (s). *Anal.* Calc. for $C_{27}H_{30}Cl_2FeN_4$ (536.1): C, 60.35; H, 5.63; N, 10.43. Found: C, 60.37; H, 5.59; N, 10.08%.

Data for **Fe4** are as follows. Yield: 83.4%. IR (KBr; cm^{-1}): 3449.7 (m), 3082.6 (w), 1592.3 (vs), 1476.3 (s), 1320.9 (s), 1213.5 (s), 854.5 (s), 788.9 (s), 746.8 (s). *Anal.* Calc. for $C_{24}H_{24}Cl_2FeN_4$ (494.2): C, 58.21; H, 4.88; N, 11.31. Found: C, 58.33; H, 5.01; N, 11.17%.

Data for **Fe5** are as follows. Yield: 81.0%. IR (KBr; cm^{-1}): 3423.9 (m), 3051.9 (m), 2966.3 (m), 1600.9 (vs), 1568.6 (m), 1460.2 (s), 1417.5 (m), 1318.3 (s), 1213.8 (s), 858.4 (m), 786.2 (m), 746.2 (s). *Anal.* Calc. for $C_{26}H_{28}Cl_2FeN_4$ (522.1): C, 59.68; H, 5.39; N, 10.71. Found: C, 59.33; H, 5.43; N, 10.50%.

Data for **Fe6** are as follows. Yield: 77.6%. IR (KBr; cm^{-1}): 3418.4 (w), 3058.2 (m), 1600.9 (vs), 1478.4 (m), 1436.3 (s), 1318.9 (s), 1043.9 (m), 978.4 (m), 773.6 (m), 791.4 (m). *Anal.* Calc. for $C_{21}H_{16}Cl_4FeN_4$ (519.9): C, 48.32; H, 3.09; N, 10.73. Found: C, 48.39; H, 2.89; N, 10.50%.

Data for **Fe7** are as follows. Yield: 90.3%. IR (KBr; cm^{-1}): 3343.9 (m), 3058.2 (m), 1597.0 (vs), 1476.3 (m), 1423.8 (m), 1315.3 (s), 1210.7 (m), 923.5 (m), 809.7 (m), 745.6 (s). *Anal.* Calc. for $C_{22}H_{19}Cl_3FeN_4$ (500.0): C, 52.68; H, 3.82; N, 11.17. Found: C, 52.49; H, 3.55; N, 11.25%.

Data for **Fe8** are as follows. Yield: 88.7%. IR (KBr; cm^{-1}): 3067.8 (m), 2967.5 (m), 1596.5 (vs), 1486.3 (m), 1406.3 (m), 1315.7 (s), 1204.6 (w), 1056.1 (m), 815.0 (s), 767.2 (m). *Anal.* Calc. for $C_{24}H_{23}Cl_3FeN_4$ (528.0): C, 54.42; H, 4.38; N, 10.58. Found: C, 54.52; H, 4.71; N, 10.27%.

Data for **Fe9** are as follows. Yield: 82.1%. IR (KBr; cm^{-1}): 3067.8 (m), 2967.5 (m), 1596.5 (vs), 1486.3 (m), 1406.3 (m), 1315.7 (s), 1204.6 (w), 1056.1 (m), 815.0 (s), 767.2 (m). *Anal.* Calc. for $C_{26}H_{27}Cl_3FeN_4$ (556.1): C, 55.99; H, 4.88; N, 10.05. Found: C, 55.72; H, 4.93; N, 9.83%.

Data for **Fe10** are as follows. Yield: 79.8%. IR (KBr; cm^{-1}): 3032.0 (m), 1593.8 (vs), 1480.9 (m), 1406.7 (m), 1318.1 (s), 1215.1 (s), 1019.4 (m), 925.5 (m), 848.7 (s), 809.1 (s), 740.3 (m). *Anal.* Calc. for $C_{23}H_{21}Cl_3FeN_4$ (514.0): C, 53.57; H, 4.10; N, 10.87. Found: C, 53.98; H, 4.31; N, 10.55%.

Data for **Fe11** are as follows. Yield: 78.9%. IR (KBr; cm^{-1}): 3448.4 (w), 3048.9 (m), 2968.7 (m), 1598.5 (vs), 1460.4 (m), 1410.5 (m), 1318.6 (s), 1146.8 (s), 966.4 (m), 858.6 (s), 740.3 (s). *Anal.* Calc. for $C_{25}H_{25}Cl_3FeN_4$ (542.1): C, 55.23; H, 4.63; N, 10.30. Found: C, 55.15; H, 4.77; N, 10.01%.

Data for **Fe12** are as follows. Yield: 60.2%. IR (KBr; cm^{-1}): 3437.9 (m), 3058.2 (m), 1599.7 (vs), 1557.1 (m), 1485.6 (m), 1435.1 (s), 1319.9 (s), 1130.7 (m), 977.6 (m), 863.0 (m), 814.0 (s), 791.4 (m), 659.3 (m). *Anal.* Calc. for $C_{20}H_{13}Cl_5FeN_4$ (539.9): C, 44.28; H, 2.42; N, 10.33. Found: C, 44.40; H, 2.51; N, 10.36%.

4.3. Procedure for ethylene oligomerization

Ethylene oligomerization was performed in a stainless steel autoclave (0.5 L capacity) equipped with a gas ballast through a solenoid clave for continuous feeding of ethylene at constant pressure. A 100 mL amount of toluene containing the catalyst precursor and the required amount of co-catalyst was transferred into the fully dried reactor via a syringe under a nitrogen atmosphere. At the reaction temperature, the reactor was sealed and pressurized to high ethylene pressure, and the ethylene pressure was maintained during feeding of ethylene. After the reaction mixture was stirred for the desired period, the pressure was released and a small amount of the reaction solution was collected, which was then analyzed by gas chromatography (GC) to determine the composition and mass distribution of the oligomers obtained. To keep the reaction temperature constant, the autoclave is equipped with inert heat exchange tube of water.

4.4. X-ray crystallographic studies

Single-crystals of **Fe2** and **Fe3** suitable for X-ray diffraction were obtained by slow diffusion of diethyl ether into methanol solution. Data were collected with a Rigaku RAXIS Rapid IP diffractometer with graphite monochromated Mo Kα radiation ($\lambda = 0.71073$ Å). Cell parameters were obtained by global refinement of the positions of all collected reflections. Intensities were corrected for Lorentz and polarization effects and empirical absorption. The structures were solved by direct methods and refined by full-matrix least squares on F^2. All non-hydrogen atoms were refined anisotropically. All hydrogen atoms were placed in calculated positions. Structure solution and refinement were performed by using the SHELXL-97 package [50]. Crystal data and processing parameters for **Fe2** and **Fe3** are summarized in Table 4.

Acknowledgments

This work is supported by MOST 863 Program No. 2009AA0 33601 and NSFC No. 21072120.

Appendix A. Supplementary material

CCDC **812006** and **812007** contain the supplementary crystallographic data for **Fe2** and **Fe3**. These data can be obtained free of charge from The Cambridge Crystallographic Data Centre via www.ccdc.cam.ac.uk/data_request/cif. Supplementary data associated with this article can be found, in the online version, at doi:10.1016/j.ica.2011.09.035.

References

[1] V.C. Gibson, S.K. Spitzmesser, Chem. Rev. 103 (2003) 283.
[2] G.J.P. Britovsek, V.C. Gibson, D.F. Wass, Angew. Chem., Int. Ed. 38 (1999) 428.
[3] S.D. Ittel, L.K. Johnson, M. Brookhart, Chem. Rev. 100 (2000) 1169.
[4] C. Bianchini, G. Giambastiani, I.G. Rios, G. Mantovani, A. Meli, A.M. Segarra, Coord. Chem. Rev. 250 (2006) 1391.
[5] V.C. Gibson, C. Redshaw, G.A. Solan, Chem. Rev. 107 (2007) 1745.
[6] W.-H. Sun, S. Zhang, W. Zuo, C. R. Chim. 11 (2008) 307.
[7] C. Bianchini, G. Giambastiani, L. Luconi, A. Meli, Coord. Chem. Rev. 254 (2010) 431.
[8] S. Jie, W.-H. Sun, T. Xiao, Chin. J. Polym. Sci. 28 (2010) 299.
[9] A.M.A. Bennett (Dupont), PCT Int. Appl. WO9827124 Al, 1998 (priority date 17.12.1996).
[10] B.L. Small, M. Brookhart, A.M.A. Bennett, J. Am. Chem. Soc. 120 (1998) 4049.
[11] G.J.P. Britovsek, V.C. Gibson, B.S. Kimberley, P.J. Maddox, S.J. McTavish, G.A. Solan, A.J.P. White, D.J. Williams, Chem. Commun. (1998) 849.
[12] B.L. Small, M. Brookhart, J. Am. Chem. Soc. 120 (1998) 7143.
[13] G.J.P. Britovsek, M. Bruce, V.C. Gibson, B.S. Kimberley, P.J. Maddox, S. Mastroianni, S.J. McTavish, C. Redshaw, G.A. Solan, S. Strömberg, A.J.P. White, D.J. Williams, J. Am. Chem. Soc. 121 (1999) 8728.
[14] Y. Chen, C. Qian, J. Sun, Organometallics 22 (2003) 1231.
[15] C. Bianchini, D. Gatteschi, G. Giambastiani, I.G. Rios, A. Ienco, F. Laschi, C. Mealli, A. Meli, L. Sorace, A. Toti, F. Vizza, Organometallics 26 (2007) 726.
[16] P. Barbaro, C. Bianchini, G. Giambastiani, I.G. Rios, A. Meli, W. Oberhauser, A.M. Segarra, L. Sorace, A. Toti, Organometallics 26 (2007) 4639.
[17] Z. Ma, W.-H. Sun, Z. Li, C. Shao, Y. Hu, X. Li, Polym. Int. 51 (2002) 994.
[18] B.L. Small, Organometallics 22 (2003) 3178.
[19] B.L. Small, M.J. Carney, D.M. Holman, C.E. O'Rourke, J.A. Halfen, Macromolecules 37 (2004) 4375.
[20] C. Wallenhorst, G. Kehr, H. Luftmann, R. Fröhlich, G. Erker, Organometallics 27 (2008) 6547.
[21] L. Guo, H. Gao, L. Zhang, F. Zhu, Q. Wu, Organometallics 29 (2010) 2118.
[22] J. Yu, H. Liu, W. Zhang, X. Hao, W.-H. Sun, Chem. Commun. 47 (2011) 3257.
[23] Q.-Z. Yang, A. Kermagoret, M. Agostinho, O. Siri, P. Braunstein, Organometallics 25 (2006) 5518.
[24] F. Speiser, P. Braunstein, L. Saussine, Dalton Trans. 23 (2004) 1539.
[25] J. Hou, W.-H. Sun, S. Zhang, H. Ma, Y. Deng, X. Lu, Organometallics 25 (2006) 236.
[26] C. Zhang, W.-H. Sun, Z.-X. Wang, Eur. J. Inorg. Chem. 23 (2006) 4895.
[27] S. Al-Benna, M.J. Sarsfield, M. Thornton-Pett, D.L. Ormsby, P.J. Maddox, P. Brés, M. Bochmann, J. Chem. Soc., Dalton Trans. 23 (2000) 4247.
[28] A.P. Armitage, Y.D.M. Champouret, H. Grigoli, J.D.A. Pelletier, K. Singh, G.A. Solan, Eur. J. Inorg. Chem. 29 (2008) 4597.
[29] F.A. Kunrath, R.F. Souza, O.L. Casagrande Jr., N.R. Brooks, V.G. Young Jr., Organometallics 22 (2003) 4739.
[30] N. Ajellal, M.C.A. Kuhn, A.D.G. Boff, M. Ĥorner, C.M. Thomas, J.-F. Carpentier, O.L. Casagrande Jr., Organometallics 25 (2006) 1213.
[31] W.-H. Sun, S. Jie, S. Zhang, W. Zhang, Y. Song, H. Ma, J. Chen, K. Wedeking, R. Fröhlich, Organometallics 25 (2006) 666.
[32] S. Jie, S. Zhang, W.-H. Sun, X. Kuang, T. Liu, J. Guo, J. Mol. Catal. A: Chem. 269 (2007) 85.
[33] S. Jie, S. Zhang, W.-H. Sun, Eur. J. Inorg. Chem. 35 (2007) 5584.
[34] M. Zhang, P. Hao, W. Zuo, S. Jie, W.-H. Sun, J. Organomet. Chem. 693 (2008) 483.
[35] M. Zhang, R. Gao, X. Hao, W.-H. Sun, J. Organomet. Chem. 693 (2008) 3867.
[36] W.-H. Sun, P. Hao, G. Li, S. Zhang, W. Wang, J. Yi, M. Asma, N. Tang, J. Organomet. Chem. 692 (2007) 4506.
[37] W.-H. Sun, P. Hao, S. Zhang, Q. Shi, W. Zuo, X. Tang, X. Lu, Organometallics 26 (2007) 2720.
[38] Y. Chen, P. Hao, W. Zuo, K. Gao, W.-H. Sun, J. Organomet. Chem. 693 (2008) 1829.
[39] L. Xiao, R. Gao, M. Zhang, Y. Li, X. Cao, W.-H. Sun, Organometallics 28 (2009) 2225.
[40] K. Wang, K. Wedeking, W. Zuo, D. Zhang, W.-H. Sun, J. Organomet. Chem. 693 (2008) 1073.
[41] S. Zhang, I. Vystorop, Z. Tang, W.-H. Sun, Organometallics 26 (2007) 2456.
[42] W.-H. Sun, K. Wang, K. Wedeking, D. Zhang, S. Zhang, J. Cai, Y. Li, Organometallics 26 (2007) 4781.
[43] X. Chen, L. Zhang, T. Liang, X. Hao, W.-H. Sun, C. R. Chim. 13 (2010) 1450.
[44] X. Chen, L. Zhang, J. Yu, X. Hao, H. Liu, W.-H. Sun, Inorg. Chim. Acta 370 (2011) 156.
[45] G.V.Z. Schulz, Phys. Chem. Abt. B 30 (1935) 379.
[46] G.V.Z. Schulz, Phys. Chem. Abt. B 43 (1939) 25.
[47] P.J. Flory, J. Am. Chem. Soc. 62 (1940) 1561.
[48] G. Henrici-Olivé, S. Olivé, Adv. Polym. Sci. 15 (1974) 1.
[49] E.Y. Chen, T.J. Marks, Chem. Rev. 100 (2000) 1391.
[50] G.M. Sheldrick, SHELXTL-97, Program for the Refinement of Crystal Structures, University of Göttingen, Germany, 1997.